ELSEVIER

Carbohydrate Research 337 (2002) 2279–2299

CARBOHYDRATE RESEARCH

www.elsevier.com/locate/carres

Conformational analysis of two xylose-containing N-glycans in aqueous solution by using ^{1}H NMR ROESY and NOESY spectroscopy in combination with MD simulations

Jos P.M. Lommerse,[a] Johannes J.M. van Rooijen,[a] Loes M.J. Kroon-Batenburg,[b] Johannis P. Kamerling,[a] Johannes F.G. Vliegenthart[a,*]

[a] *Bijvoet Center, Department of Bio-Organic Chemistry, Section of Glycoscience and Biocatalysis, Utrecht University, Padualaan 8, NL-3584 CH Utrecht, The Netherlands*

[b] *Bijvoet Center, Department of Crystal and Structural Chemistry, Utrecht University, Padualaan 8, NL-3584 CH Utrecht, The Netherlands*

Received 15 May 2002; accepted 11 July 2002

Dedicated to Professor Derek Horton on the occasion of his 70th birthday

Abstract

The conformational behavior of the synthetic hexa- and heptasaccharide methyl β-glycosides α-D-Man*p*-(1→6)-[α-D-Man*p*-(1→3)-][β-D-Xyl*p*-(1→2)-]β-D-Man*p*-(1→4)-β-D-Glc*p*NAc-(1→4)-β-D-Glc*p*NAc-(1→OMe and α-D-Man*p*-(1→6)-[α-D-Man*p*-(1→3)-][β-D-Xyl*p*-(1→2)-]β-D-Man*p*-(1→4)-β-D-Glc*p*NAc-(1→4)-[α-L-Fuc*p*-(1→6)-]β-D-Glc*p*NAc-(1→OMe, representing the xylosylated and the xylosylated α-(1→6)-fucosylated core structures of N-glycans in α_D-hemocyanin of the snail *Helix pomatia*, respectively, were investigated by ^{1}H NMR spectroscopy in combination with molecular dynamics (MD) simulations in water. ^{1}H and ^{13}C chemical shifts of the oligosaccharides were assigned using ^{1}H–^{1}H COSY, TOCSY, and NOESY, and ^{1}H–^{13}C HMQC techniques. Experimental 2D ^{1}H cross-peak intensities from one series of NOESY and one series of ROESY experiments of the two oligosaccharides were compared with calculated values derived from MD trajectories using the CROSREL program, yielding information about the conformation of each glycosidic linkage of the methyl glycosides. The flexibility of the linkages was described by generalized order parameters and internal rotation correlation times. Analysis of the data indicated that several conformations are likely to exist for the α-D-Man-(1→6)-β-D-Man, the α-L-Fuc-(1→6)-β-D-GlcNAc, and the α-D-Man-(1→3)-β-D-Man linkage, whereas the β-D-Xyl-(1→2)-β-D-Man-(1→4)-β-D-GlcNAc-(1→4)-β-D-GlcNAc fragment occurs in one rigid conformation. No significant differences were found between the corresponding structural elements in both methyl glycosides. NOESY and ROESY experiments proved to be suitable for providing the experimental data required, however, due to more overlap within the ROESY spectra, reducing the accuracy of the analysis, NOESY spectral analysis is preferred.

Keywords: Glycoprotein; Glycan; Conformational analysis; NMR spectroscopy; Molecular mechanics; Molecular dynamics

1. Introduction

In recent years, considerable progress has been made in the conformational analysis of glycoprotein glycans, both by improved experimental techniques and by more accurate theoretical methods.[1–5] The analysis is usually focused on defining the dihedral angles of the glycosidic linkages (ϕ and ψ) and of the exocyclic-substituted oxymethyl groups (ω). An 'ensemble' of conformations might be present, which consists of a number of energetically favorable conformations that coexist in solution. Conformational analysis of large glycans can yield additional data, like long-distance effects between their atoms. More importantly, the conformations and internal flexibilities of these intact glycans might deviate from the sum of the disaccharide building blocks.

* Corresponding author. Tel.: +31-30-2532281; fax: +31-30-2540980

E-mail address: j.f.g.vliegenthart@chem.uu.nl (J.F.G. Vliegenthart).

0008-6215/02/$ - see front matter
PII: S0008-6215(02)00212-4

^{1}H nuclear Overhauser enhancement NMR spectroscopy (NOESY) is often the method of choice to obtain experimental data for biomolecules in aqueous solution, providing data related to distances between protons. However, for small biomolecules NOESY will hardly be applicable as the rotational frequency of the molecule causes the nuclear Overhauser enhancement to be close to zero. This problem can be overcome using a modified nOe experiment, i.e., rotating frame nuclear Overhauser enhancement spectroscopy (ROESY). Typical examples of a disaccharide and tetrasaccharides can be found in Refs. 6 and 7.

Molecular dynamics (MD) simulations can be performed to obtain theoretical models for oligosaccharides. Using the CROSREL program,[8] nOe and rOe intensities are calculated for theoretical models and these intensities are compared with experimental values from NOESY and ROESY spectra, respectively. Calculation of rOe intensities from interproton distances is relatively complex in comparison with nOe intensities, because factors as offset dependency, spin-lock field strength, and TOCSY transfers have to be taken into account.[9] However, it is possible to deal with such factors, and spectra can be analyzed in terms of conformations and of internal motions of the molecule.[10]

In this study, the conformational analysis of the hexa- and heptasaccharide methyl β-glycosides **1** and **2**, representing the xylose-containing low-molecular mass N-glycans of α_D-hemocyanin of the snail *Helix pomatia*[11,12] is presented. As these methyl glycosides have the proper size to gain experimental data from NOESY, as well as from ROESY spectroscopy, both methods were tested and compared for their applicability in conformational analysis.

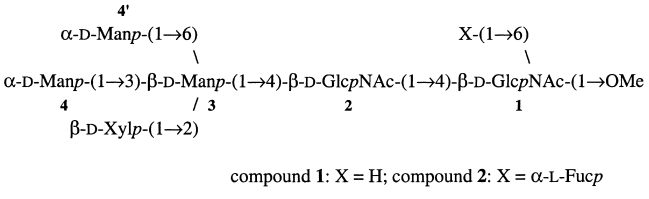

compound **1**: X = H; compound **2**: X = α-L-Fuc*p*

2. Materials and methods

Materials.—The methyl glycosides **1** and **2**[13] were kindly donated by Dr J.G.M. van der Ven (Department of Bio-Organic Chemistry, Utrecht University).

^{1}H and ^{13}C NMR spectroscopy.—Compounds **1** and **2** were exchanged twice in D_2O (99.9% D, MSD Isotopes), with intermediate lyophilization, then dissolved in 450 μL D_2O (99.96% D, MSD Isotopes). 500 MHz 1D/2D ^{1}H NMR measurements were carried out on a Bruker AMX-500 spectrometer (Bijvoet Center, Department of NMR Spectroscopy, Utrecht University) at a probe temperature of 282 K. Suppression of the HOD signal was performed by presaturation during the relaxation delay for 1 s. ^{1}H chemical shifts (δ) are given in ppm relative to the signal for internal sodium 4,4-dimethyl-4-silapentane-1-sulfonate, but were actually measured by reference to the signal for internal acetone (δ 2.225).[14] All 2D data matrices were processed on a Silicon Graphics 3D/35 computer using the TRITON software (R. Kaptein and R. Boelens, Department of NMR Spectroscopy, Utrecht University).

2D TOCSY experiments were recorded using MLEV-17 mixing sequence cycles[15] at an effective field strength of 9 kHz and with the offset frequency placed on the HOD frequency position. The mixing time for **1** was 120 ms and the spectrum was recorded at a spectral width of 3200 Hz in each dimension. The mixing time for **2** was 100 ms and the spectrum was recorded at a spectral width of 3520 Hz in each dimension. Each TOCSY experiment consisted of a 512×4 K data matrix, which was zero filled and multiplied by a $\pi/4$ shifted sine-bell prior to Fourier transformation, resulting in a 1 K $\times$ 4 K spectral data matrix.

2D NOESY spectra[16] were recorded using mixing times of 75, 150, 250, 375 or 525 ms, respectively, for both **1** and **2**. The carrier was placed on the HOD resonance frequency and the spectral width was set 5000 Hz for both compounds. The obtained 512×4 K data matrices were zero filled and multiplied by a $\pi/3$ shifted sine-bell prior to Fourier transformations resulting in 2 K $\times$ 4 K spectral data matrices. Peak intensities were determined by integration in a rectangular area around the peak maximum, or, in the case of overlap, around the center of the peak cluster. A correction for the local base-line area was performed by subtracting an average of identical integrated rectangular areas around the cross-peak location.

2D ROESY spectra[17] of both **1** and **2** were recorded using spin-lock times of 25, 50, 80, 115, 145 or 200 ms, respectively, at a field strength of 2.2 kHz, having the carrier frequency low field outside the ^{1}H spectrum at δ 5.93. In the case of **1**, the spectral width was 4000 Hz in each dimension, whereas for **2** this value was 5000 Hz. Fourier transformations and peak integration were performed as described for the NOESY experiments.

A DQF ^{1}H–^{1}H COSY[18] spectrum of **1** was recorded using a spectral width of 3200 Hz. The 512×4 K data matrix was zero filled and multiplied by a $\pi/4$ shifted sine-bell prior to Fourier transformation, resulting in a 1 K $\times$ 4 K spectral data matrix.

Natural abundance 1D ^{1}H-decoupled ^{13}C measurements were carried out on a Bruker AC-300 spectrometer operating at 75 MHz at 300 K. ^{13}C Chemical shifts (δ) are given in ppm relative to the signal for external Me_4Si, but were actually measured by reference to the signal for internal acetone (δ 31.55).

A $^{1}H-^{13}C$ HMQC experiment[19] was carried out for **2** at 500 MHz for the ^{1}H and at 126 MHz for the ^{13}C nuclei, using spectral widths of 4032 and 25,120 Hz, respectively. The pulse sequence suppressed effectively the unwanted signals from protons that are not coupled to ^{13}C nuclei by a BIRD pulse sequence.[20] ^{13}C decoupling was not applied during acquisition of the ^{1}H FID. A 413×2 K data matrix was obtained. The number of data points in the t_1 direction was extended to 550 by linear prediction,[21,22] in order to improve the resolution of the ^{13}C spectrum. Zero-filling and multiplication by a $\pi/3$ shifted sine-bell resulted in a 2 K $\times$ 2 K spectral data matrix.

HSEA calculations.—HSEA energy calculations were performed using the GEGOP program[23] on a μVAX/VMS computer. This force field only calculates the non-bonded interactions as expressed by the Kitaigorodsky energy function,[24] and accounts for the exo-anomeric effect by an additional energy term. No solvent molecules are included. The monosaccharide rings are kept rigid according to coordinates taken from X-ray data. The dihedral angles of the glycosidic bonds (ϕ and ψ) and the oxymethyl groups (ω) are the only variables. These angles are defined according to the IUPAC recommendations,[25] namely, $\phi = \theta$(O-5_A–C-1_A–O-x_B–C-x_B) and $\psi = \theta$(C-1_A–O-x_B–C-x_B–C($x-1$)$_B$), but ω is defined by θ(O-6–C-6–C-5–O-5) in this study. The glycosidic bond angles τ (C-1_A–O-x_B–C-x_B) were set to 117°.

HSEA ϕ,ψ iso-energy contour plots ('rigid maps[26,27]) were calculated for the glycosidic linkages by making steps of 5° in ϕ and ψ of the disaccharides, and were plotted at intervals of 1.5 kcal/mol with respect to the calculated global energy minimum of each constituting disaccharide.

Molecular dynamics simulations.—Molecular dynamics (MD) simulations were carried out on a Silicon Graphics 4D/35 computer, using the GROMOS program package,[28] taking parameters for the methyl glycosides as described previously.[10,29] The methyl glycoside was placed in the center of a truncated octahedron, with a minimum distance of 0.8 nm to the edges of the box. Subsequently, the octahedron was filled with 600–850 water molecules and during the simulations, the water molecules were kept rigid using the SHAKE method.[30] After energy minimization of the whole system, the simulations were started, taking initial velocities from a Maxwellian distribution, and continued with time steps of 2 fs at 282 K, and at 1 atm ($\tau_{t(solvent)} = 0.5$ ps, $\tau_{t(solute)} = 2.5$ ps, and $\tau_p = 0.5$ ps). A total-energy equilibrium of each MD simulation was reached in about 10 ps, and from 20 ps onwards, data were collected for analysis. The positions of the hydrogen atoms of the united CH, CH_2 and CH_3 atoms were calculated after the simulation, using 'perfect' tetrahedral geometries and C–H bond lengths of 0.11 nm.

For **1**, two long MD simulations A and B (520 ps each) were performed, starting with the lowest energy conformations from HSEA calculations. Run A was started in the *gt* conformation of the oxymethyl group ($\omega = 60°$) of Man-**3** and run B in the corresponding *gg* rotamer ($\omega = -60°$). In a similar way, four long MD simulations were performed for **2**. Runs A, B, C and D of **2** (600, 200, 300 and 100 ps, respectively) were started with the lowest energy conformations for the rotamers Man-**3** *gt*/GlcNAc-**1** *gg*, Man-**3** *gg*/GlcNAc-**1** *gt*, Man-**3** *gg*/GlcNAc-**1** *gg* and Man-**3** *gt*/GlcNAc-**1** *gt*, respectively.

Two criteria were applied to establish hydrogen bond formation during the MD simulations: (1) a distance of less than 0.24 nm between the donor hydrogen atom and the acceptor; (2) a hydrogen bond angle of more than 120°.[31]

Theoretical models of the methyl glycoside conformations consisted of $^{1}H-^{1}H$ distance matrices, calculated by $r = \langle r^{-3} \rangle^{-1/3}$ for each complete MD trajectory. The distance matrices of **1** and **2** were formed by 50 and 58 protons, respectively. The distance matrices of the trajectories A and B of **1** were combined (model A/B) to obtain one average model for the *gg* and *gt* rotamers of the α-D-Man-(1→6)-β-D-Man linkage. Similarly, one model for the rotamers of both the α-D-Man-(1→6)-β-D-Man and the α-L-Fuc-(1→6)-β-D-GlcNAc linkages was constructed by combining the distance matrices of trajectories A, B, C and D of **2** (model A/B/C/D). Combination of distance matrices was performed by $r = [\Sigma\, w_k \cdot r^{-6}]^{-1/6}$, in which the normalized weights w_k for each distance matrix k were calculated according to the rotamer distributions and the lengths of the trajectories.

The generalized order parameters, S_f^2, for the long MD trajectories were calculated from internal rotation correlation function plots as described, using average plateau values between 15 and 20 ps.[10] S_f^2 values for the combined models A/B of **1** and A/B/C/D of **2** were calculated by $S_f^2 = \Sigma\, w_k \cdot S_f^2$.

NOESY and ROESY spectra analysis.—The principles of NOESY and ROESY spectra analysis in the CROSREL program have been described earlier,[8] and include a treatment for TOCSY effects occurring in ROESY experiments. The experimental nOe or rOe data were transferred into matrices, in which each column (ω_2 constant) was scaled according to $\mathbf{M}_0$-scaling.[8] In order to determine the nOe, and, in a different way, rOe build up rates, a method was applied, which includes descriptions of motions occurring within the oligosaccharide chain, like the generalized order parameters, S_f^2, and the local rotation correlation time, τ_k (method IV in Ref. 10).

Rotation correlation times were determined for each theoretical model by fitting calculated intraresidual $^{1}H-^{1}H$ nOe's or rOe's to the experiment. For consistency,

the same $^1H-^1H$ pairs in the NOESY and ROESY spectra were used. Those intraresidual $^1H-^1H$ pairs were taken, in which one of the protons is an anomeric proton. Furthermore, the intraresidual $^1H-^1H$ pairs were preferably chosen in a non-overlapping part of the spectrum, without the presence of strong TOCSY relay effects in the ROESY spectra, and in particular, without overlapping interresidual $^1H-^1H$ pairs.

The R_w value was used to evaluate the fit of a set of calculated nOe's and rOe's to the experimental data.[8]

Characteristic times for glycosidic conformational transitions are calculated from local rotation correlation times of the monosaccharides of the oligosaccharide chain involved.[10] The motion of a certain monosaccharide residue k is regarded as an addition of the motion of the flexible glycosidic linkage k to the motion of a less mobile, preceding residue $(k-1)$ being closer to the center of mass. As a result, the monosaccharide residue more remote from the center of mass will have a smaller rotation correlation time:

$$\tau^1_k = \tau^1_{k-1} + \tau^1_{s,k} \quad (1)$$

The slow-internal rotation correlation time $\tau_{s,k}$ is associated with the frequency of large transitions of the glycosidic linkages.[10] A small $\tau_{s,k}$ value points to a high transition rate between the various energy minimum regions in the ϕ,ψ space of a glycosidic linkage.

In order to get an overview of the conformational space accessible, nOe or rOe 'ovals' were calculated as follows. Starting with the lowest energy geometries for **1** and **2** as determined by HSEA calculations, ϕ and ψ of each glycosidic linkage were varied in steps of 20°. For each obtained geometric HSEA model, the nOe and rOe matrices were calculated, applying the described method (Method IV in Ref. 10), using rotation correlation times and generalized order parameters of the combined models A/B (compound **1**) or A/B/C/D (compound **2**). The obtained 18×18 nOe and rOe matrices were used to calculate ϕ,ψ ovals for individual interresidual $^1H-^1H$ pairs, on which the R_w value $= 0$ (exact fit to the experimental data).

3. Results and discussion

^1H and ^{13}C chemical shift assignments.—The ^1H NMR chemical shift values of methyl glycoside **1** are listed in Table 1. The signals of the anomeric protons and the *N*-acetyl methyl groups were assigned by comparison with the ^1H NMR data of the free N-glycan released from α_D-hemocyanin.[12] The Xyl H-1 and GlcNAc-**1** H-1 doublets partially overlap, and were verified by 2D NMR analysis. The assignment of all remaining protons is based on 2D TOCSY, 2D COSY, 2D

Table 1
^1H NMR chemical shift values (ppm) of compound **1** and compound **2** at 282 K

Proton	Man-**4′**	Man-**4**	Xyl	Man-**3**	GlcNAc-**2**	GlcNAc-**1**	Fuc
Residues of compound ***1***							
H-1	4.913	5.115	4.436	4.882	4.594	4.425	
H-2	3.983	4.033	3.377	4.273	3.792	3.727	
H-3	3.852	3.827	3.437	3.873	3.753	3.678	
H-4	3.644	3.632	3.631	3.804	3.734	3.622	
$H\text{-}5_{ax}$	3.640	3.998	3.250	3.675	3.636	3.519	
$H\text{-}5_{eq}$			3.968				
H-6pro*S*	3.887	3.911		3.762	3.875	3.870	
H-6pro*R*	3.754	3.714		3.968	3.76	3.671	
NAc					2.078 [a]	2.029 [a]	
OMe						3.495	
Residues of compound ***2***							
H-1	4.912	5.116	4.441	4.883	4.672	4.425	4.905
H-2	3.981	4.032	3.378	4.273	3.784 [b]	3.735	3.801
H-3	3.853	3.827	3.458	3.871	3.745 [b]	3.665	3.938
H-4	3.651	3.634	3.710	3.799	3.721	3.811	3.816
$H\text{-}5_{ax}$	3.627 [b]	3.984	3.255	3.678	3.624	3.634	4.137
$H\text{-}5_{eq}$			4.018				
H-6pro*S*	3.884 [b]	3.911		3.765	3.874	3.958	
H-6pro*R*	3.761 [b]	3.715		3.965	3.730 [b]	3.656	
NAc/CH_3					2.088 [a]	2.030 [a]	1.235 [a]
OMe						3.487	

[a] Chemical shift value obtained from 1D experiment at 300 K.
[b] Chemical shift value obtained from HMQC experiments at 300 K.

Table 2
^{13}C NMR chemical shift values (ppm) of compound **1** and compound **2** at 300 K

Carbon	Man-**4′**	Man-**4**	Xyl	Man-**3**	GlcNAc-**2**	GlcNAc-**1**	Fuc
Residues of compound ***1***							
C-1	100.92	103.52	106.35	101.83	102.62	103.14	
C-2	71.12	71.27	74.64	80.55 [b]	56.31	56.20	
C-3	71.80	71.63	76.68	78.63	73.34	73.85	
C-4	68.02	68.07	70.60	67.78	80.84 [a]	80.63 [a]	
C-5	74.02	74.86	66.23	75.71 [b]	75.71 [b]	75.84 [b]	
C-6	62.22	62.55		66.67	61.41	61.41	
$COCH_3$					175.98	175.98	
$COCH_3$					23.46	23.46	
OMe						58.41	
Residues of compound ***2***							
C-1	100.92	103.49	106.35	101.83	102.30	103.20	100.70
C-2	71.10	71.25	74.63	80.58	56.29	56.24	69.43
C-3	71.77	71.60	76.61	78.58	73.36	73.74	70.78
C-4	67.99	68.04	70.57	67.78	80.93	79.85	73.13
C-5	74.00	74.83	66.20	75.68	74.75	75.68	68.09
C-6	62.20	62.51		66.68	61.35	67.70	
$COCH_3$					175.93	175.93	
$COCH_3/CH_3$					23.58	23.45	16.62
OMe						58.29	

Carbon chemical shift values with superscript [a] or [b] possibly have to be interchanged.

ROESY, and 2D NOESY experiments. The stereospecific assignments of the H-6pro*S* and H-6pro*R* signals were performed with guidance of ^1H NMR data from studies on stereospecifically deuterated D-hexopyranoses.[32] For the correct assignment of Man-**3** H-6pro*S* and Man-**3** H-6pro*R*, the ^1H NMR data of the stereospecifically deuterated methyl glycoside α-D-Man-(1→6)-β-D-Man-(1→OMe[33] were essential. Assuming that the *tg* rotamer (ω = 180°) at Man-**3** does not appear, the coupling constants $^3J_{5,6proS}$ (2.7 ± 0.2 Hz) and $^3J_{5,6proR}$ (3.8 ± 0.2 Hz) point to a rotamer distribution of *gg* (ω = −60°):*gt* (ω = 60°) = 7:3, as calculated by use of a generalized Karplus equation.[34] The chemical shift values of all protons of the terminal α-D-Man-(1→6)-[α-D-Man-(1→3)-][β-D-Xyl-(1→2)-]β-D-Man fragment are similar to those reported for this terminal tetrasaccharide fragment as part of a free N-glycan, additionally α-(1→3)-fucosylated at GlcNAc-**1**.[35]

The ^1H NMR chemical shift values of **2** are listed in Table 1. The signals of the anomeric protons and the *N*-acetyl methyl groups were assigned by comparison with the ^1H NMR data of the free N-glycan released from α_D-hemocyanin.[12] The Xyl H-1 and GlcNAc-**1** H-1 doublets partially overlap, and were verified by 2D NMR analysis. The assignment of all remaining protons is based on 2D TOCSY, 2D HMQC, 2D ROESY, and 2D NOESY experiments. The $^3J_{5,6proS}$ (2.8 ± 0.2 Hz) and $^3J_{5,6proR}$ (4.0 ± 0.2 Hz) values for Man-**3** point to a rotamer distribution *gg*:*gt* = 7:3 for the Man-**4′**-α-(1→6)-Man-**3** linkage, thus identical to that found in **1**. The stereospecific assignments of GlcNAc-**1** H-6pro*S* and H-6pro*R* were accomplished by analogy with the assignments for α-D-Man-(1→6)-β-D-Man-(1→OMe.[33] In the latter case, the β-D-Man H-6 signal at lower field is assigned to H-6pro*R*. This downfield position is caused by deshielding of H-6pro*R* due to the close proximity of the ring oxygen of α-D-Man. When there's an α-L-Fuc-(1→6) instead of an α-D-Man-(1→6) residue, then H-6pro*S* will be deshielded, as the ring oxygen of α-L-Fuc has a mirror position in the chair conformation when compared to α-D-Man. Therefore, in the α-L-Fuc-(1→6)-GlcNAc-**1** fragment, the GlcNAc-**1** H-6pro*S* will have a larger chemical shift. The $^3J_{5,6proS}$ (1.5 ± 0.2 Hz, measured in the TOCSY spectrum) and $^3J_{5,6proR}$ (4.5 ± 0.5 Hz, measured in the HMQC spectrum) values corroborate this assignment, assuming that the *tg* conformation does not occur. This leads to the rotamer distribution *gg*:*gt* = 65:35 for the Fuc-α-(1→6)-GlcNAc-**1** linkage.

The ^{13}C NMR chemical shift values of **2** are listed in Table 2. The assignments of the signals are based on HMQC experiments. The ^{13}C chemical shift values of the terminal tetrasaccharide are consistent with those reported for this terminal fragment as part of a free N-glycan, additionally α-(1→3)-fucosylated at GlcNAc-**1**.[35] The ^{13}C chemical shifts of α-L-Fuc are similar to those reported for α-L-Fuc in the disaccharide α-L-Fuc-(1→6)-α-D-Glc-(1→OMe.[36] Using a 1D ^{13}C spec-

trum, the ^{13}C chemical shifts of **1** have been assigned by comparison with those of **2** (Table 2). Obviously, the most striking difference with **2** was found for the GlcNAc-**1** C-6 signal ($\Delta\delta$ −6.3 ppm).

Molecular dynamics trajectories.—MD simulations were performed for **1** and **2**, in order to investigate time-averaged conformational probes, and to obtain ensemble-averaged conformations. Furthermore, flexibility within the oligosaccharide methyl glycosides can be observed directly from the MD simulations, i.e., by transitions at the glycosidic linkages and by fast reorientational motions represented by the generalized order parameter S_f^2. The ϕ,ψ dihedral angles pairs of each glycosidic linkage of all long MD trajectories are plotted in Fig. 1 for **1** and in Fig. 2 for **2**. Average dihedral angles of the complete MD trajectories are listed in Table 3 for **1** and **2**. S_f^2 values were derived from plots of rotation correlation functions, demonstrating no large differences in S_f^2 between the corresponding structural elements of **1** and **2** (data not shown). The S_f^2 values indicate that the $^1H-^1H$ pairs of the inner monosaccharide residues Man-**3** and GlcNAc-**2** are more restricted (Man-**3**: $S_f^2 \approx 0.84$; GlcNAc-**2**: $S_f^2 \approx 0.85$) than those of the outer monosaccharide residues (Xyl: $S_f^2 \approx 0.78$; Man-**4**: $S_f^2 \approx 0.77$; Man-**4′**: $S_f^2 \approx 0.68$; GlcNAc-**1**: $S_f^2 \approx 0.80$; Fuc: $S_f^2 \approx 0.77$). Especially, the interresidual $^1H-^1H$ pairs across the α-(1→6) glycosidic linkages indicate large flexibility on the picosecond time scale ($S_f^2 \approx 0.68$). In general, small S_f^2 values are indicative of short time-scale flexibility, but the reverse that large S_f^2 values are related to strong restriction, is not necessarily true.

The stabilities of the glycosidic linkage conformations, as investigated by 59 short MD simulations, are summarized in Table 4. Hydrogen bonds, which existed for more than 5% of the total simulated MD trajectories, are listed in Table 5.

nOe and rOe analysis.—Theoretical nOe and rOe intensities were calculated for the various conformational models obtained from the MD simulations, using the CROSREL program.[8] This program does not account for relay effects caused by TOCSY transfer, occurring only during spin locking in the ROESY experiments. This transfer reaches a maximum, when two spins have approximately the same chemical shift (or opposite values with respect to the offset frequency), in combination with a large joint coupling constant. Most skeleton protons of oligosaccharide chains resonate in the same chemical shift region. If these protons have large vicinal coupling constants, due to axial positions in the rings, then many strong TOCSY relay effects will arise. Therefore, assignments of overlap in the ROESY spectra were different from those occurring in the NOESY spectra. In general, more and larger groups of protons must be treated as cases of overlap in ROESY spectra rather than in NOESY spectra. Assignments of overlap are displayed in Table 6.

Rotation correlation times.—The calculated local rotation correlation times (τ_k) for each intraresidual $^1H-^1H$ pair, are given in Table 7 for **1** and **2**. The local rotation correlation times are within experimental error consistent with the model that the monosaccharide constituents have smaller rotation correlation times when they are more remote from the center of mass of the methyl glycoside, which is close to GlcNAc-**2**. Furthermore, these τ_k values are in the same range as determined from NOESY spectra for a glycopeptide of bromelain.[10] The local rotation correlation times (τ_k) mainly depend on the intraresidual $^1H-^1H$ distances deduced from the corresponding nOe or rOe cross-peak intensities used for fitting. These fitted τ_k values are not completely independent of a theoretical model of the methyl glycoside, because: (i) certain oligosaccharide chain conformations may cause monosaccharide ring deformations, thereby altering the intraresidual $^1H-^1H$ calibration distances and; (ii) in different oligosaccharide conformations, the spin diffusion pathways will alter, which also result in slight changes of the fitted τ_k values. These kinds of variations of the τ_k values are found to be reasonably small for all monosaccharide residues in **1** and **2**. However, in the case of Man-**4′**, the fitted value of τ_k has become largely dependent on the conformation of the Man-**4′**-α-(1→6)-Man-**3** linkage, due to overlap of the intraresidual Man-**4′** H-1,Man-**4′** H-2 and the Man-**4′** H-1,Man-**3** H-6pro*R* cross-peaks. There is no alternative intraresidual cross-peak available within the Man-**4′** residue, which can be used for determination of this τ_k.

Fig. 1. Plots in the ϕ,ψ surfaces of the various glycosidic linkages of compound **1**. For each glycosidic linkage has been plotted: (1) Iso-energy contour levels as obtained by HSEA calculations at intervals of 1.5 kcal/mol from the global minimum; (2) ϕ,ψ dihedral angle pairs of the MD simulations, at intervals of 0.5–2.0 ps from the MD runs, and represent approximately the *gg* and *gt* rotamer distribution of Man-**3**; (3) optimal R_w oval(s), on which the calculated interresidual rOe intensities have the smallest deviation from the experiment (see text). Due to proton resonance clusters, which are treated as overlap in the CROSREL program, more R_w ovals for each glycosidic linkage can be present (Table 9). The $^1H-^1H$ pairs responsible for the R_w ovals are displayed in the figure. The optimal R_w ovals of the NOESY experiments are represented by a solid line, those of the ROESY experiment by a dashed line. (a) β-D-Xyl-(1→2)-β-D-Man-**3**, optimal R_w oval of Xyl H-1,Man-**3** H-2; (b) α-D-Man-**4**-(1→3)-β-D-Man-**3**, optimal R_w ovals of (1) Man-**4** H-1,Man-**3** H-3/H-4 and (2) Man-**4** H-5/H-2,Man-**3** H-2; (c1,c2) α-D-Man-**4′**-(1→6)-β-D-Man-**3**, optimal R_w ovals of (1) Man-**4′** H-1,Man-**3** H-6pro*S* and (2) Man-**4′** H-1,Man-**3** H-6pro*R*/Man-**4′** H-2; (d) β-D-Man-**3**-(1→4)-β-D-GlcNAc-**2**, optimal R_w oval of Man-**3** H-1,GlcNAc-**2** H-3/H-4/H-6pro*R*; (e) β-D-GlcNAc-**2**-(1→4)-β-D-GlcNAc-**1**, optimal R_w oval of GlcNAc-**2** H-1,GlcNAc-**1** H-3/H-4/H-6pro*R*.

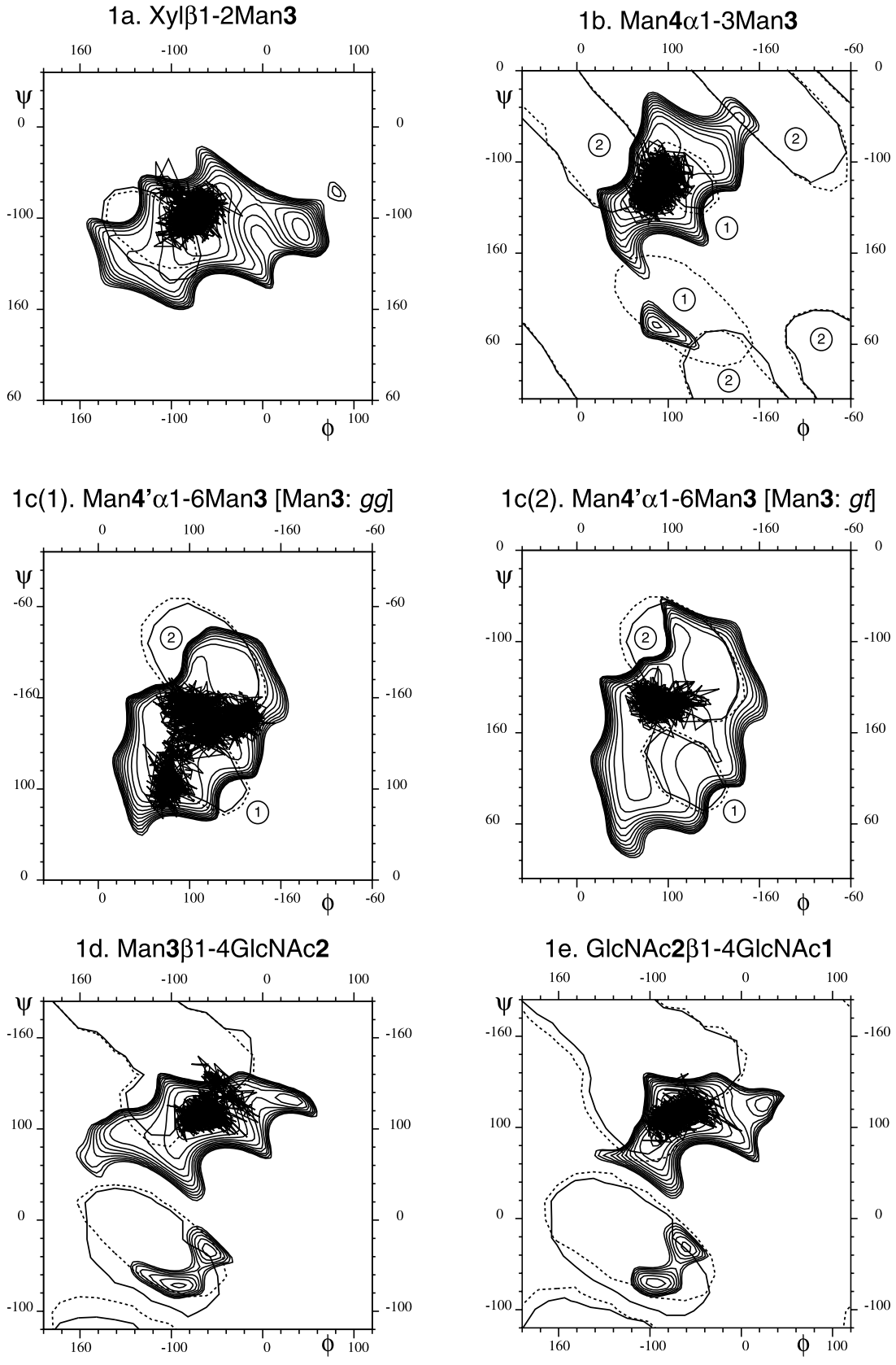
1a. Xylβ1-2Man3
1b. Man4α1-3Man3
1c(1). Man4'α1-6Man3 [Man3: gg]
1c(2). Man4'α1-6Man3 [Man3: gt]
1d. Man3β1-4GlcNAc2
1e. GlcNAc2β1-4GlcNAc1
ψ
ϕ

Fig. 1.

Table 3
Average dihedral angles of the glycosidic linkages for the complete long MD trajectories A and B of compound **1**, and A, B, C, and D of compound **2**

Traj.	t (ps)	Glycosidic linkage													
		Man-**4**′-α-(1→6)-Man-**3**			Man-**4**-α-(1→3)-Man-**3**		Xyl-β-(1→2)-Man-**3**		Man-**3**-β-(1→4)-GlcNAc-**2**		GlcNAc-**2**-β-(1→4)-GlcNAc-**1**		Fuc-α-(1→6)-GlcNAc-**1**		
		ϕ	ψ	ω	ϕ	ψ	ϕ	ψ	ϕ	ψ	ϕ	ψ	ϕ	ψ	ω
Compound ***1***															
A	500	88	−164	61	89	−119	−84	−93	−61	122	−71	113			
B	500	114	161	−60	89	−126	−75	−96	−63	116	−70	114			
Compound ***2***															
A	600	103	164	69	108	−106	−78	−100	−50	122	−59	118	−100	150	−56
B	200	95	175	−57	74	−142	−76	−105	−66	116	−65	117	−93	−154	69
C	300	104	175	−59	102	−116	−78	103	−70	112	−80	113	−93	−172	−66
D	100	104	−86	82	92	−120	−93	−105	−62	115	−82	109	−106	170	65

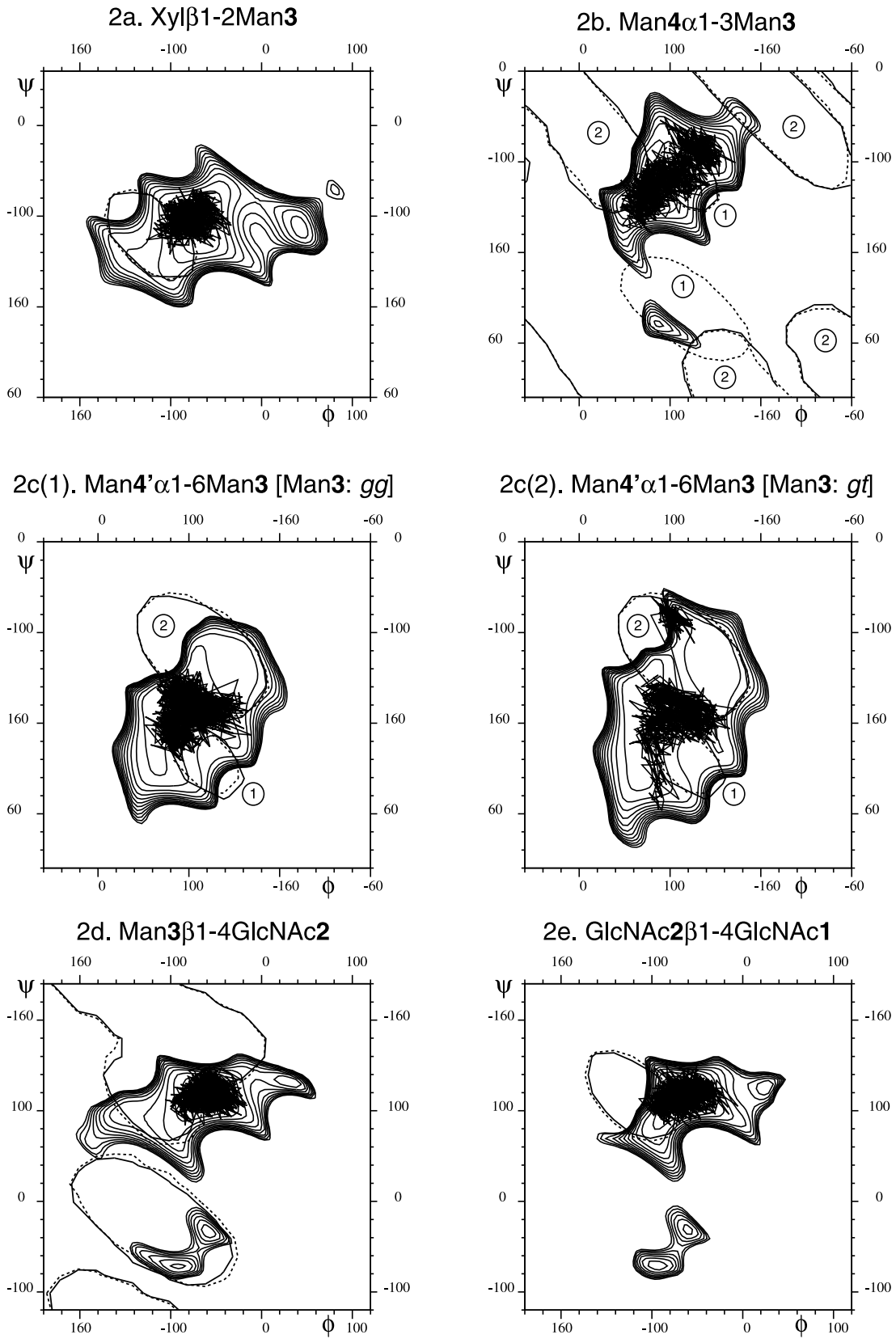
2a. Xylβ1-2Man3
2b. Man4α1-3Man3
2c(1). Man4'α1-6Man3 [Man3: gg]
2c(2). Man4'α1-6Man3 [Man3: gt]
2d. Man3β1-4GlcNAc2
2e. GlcNAc2β1-4GlcNAc1
ψ
ϕ

Fig. 2.

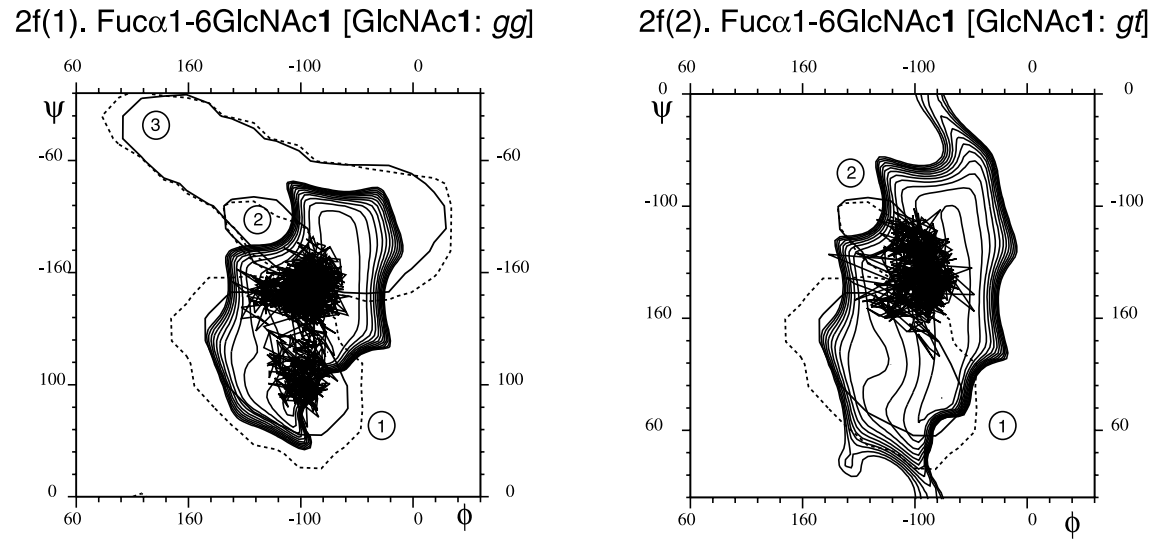

Fig. 2. Plots in the ϕ,ψ surfaces of the various glycosidic linkages of compound **2**, likewise Fig. 1, except for the ϕ,ψ dihedral angle pairs of the MD simulations, which represent approximately the *gg* and *gt* rotamer distribution of Man-**3** and GlcNAc-**1**: (a) β-D-Xyl-(1→2)-β-D-Man-**3**, optimal R_w oval of Xyl H-1,Man-**3** H-2; (b) α-D-Man-**4**-(1→3)-β-D-Man-**3**, optimal R_w ovals of (1) Man-**4** H-1,Man-**3** H-3/H-4 and (2) Man-**4** H-5/H-2,Man-**3** H-2; (c1,c2) α-D-Man-**4′**-(1→6)-β-D-Man-**3**, optimal R_w ovals of (1) Man-**4′** H-1,Man-**3** H-6pro*S* and (2) Man-**4′** H-1,Man-**3** H-6pro*R*/Man-**4′** H-2; (d) β-D-Man-**3**-(1→4)-β-D-GlcNAc-**2**, optimal R_w oval of Man-**3** H-1,GlcNAc-**2** H-3/H-4/H-6pro*R*; (e) β-D-GlcNAc-**2**-(1→4)-β-D-GlcNAc-**1**, optimal R_w oval of GlcNAc-**2** H-1,GlcNAc-**1** H-3/H-4; (f1,f2) α-L-Fuc-(1→6)-β-D-GlcNAc-**1**, optimal R_w ovals of (1) Fuc H-1,GlcNAc-**1** H-6pro*S*, (2) Fuc H-1,GlcNAc-**1** H-6pro*R*, and (3) Fuc H-1,GlcNAc-**2** H-1.

The slow-internal rotation correlation time $\tau_{s,k}$ of each glycosidic linkage is calculated according to Eq. (1), and is a measure for the flexibility of the involved linkage.[10] Similar $\tau_{s,k}$ values have been derived for the NOESY and ROESY experiments. In both **1** and **2**, the $\tau_{s,k}$ values are significantly smaller for the linkages to the oxymethyl groups [(1→6)-linkages] than for the other glycosidic linkages (Table 8). This agrees with the general opinion about flexible (1→6)-linkages.[37] It should be noted that the larger $\tau_{s,k}$ values are very sensitive to small variations in the corresponding τ_k values. For the Xyl-β-(1→2)-Man-**3** linkage rather different $\tau_{s,k}$ values have been obtained from the NOESY (2.5 and 3.0 ns for **1** and **2**, respectively) and from the ROESY (7.7 and 7.5 ns, respectively) (Table 8) experiments. This gives some uncertainty about the mobility of these linkages, but which are likely to be less mobile than the (1→6)-linkages as those have all $\tau_{s,k}$ values smaller than 2.5 ns.

Qualitative comparison with the experimental data.— The interresidual R_w values quantify the agreement of a conformation or ensemble of glycosidic conformations to the experimental data. The R_w values are listed for each individual interresidual nOe and rOe build-up curve in Table 9 for **1** and **2**. Similar R_w values have been obtained for the NOESY and ROESY spectral analyses, so in principle, both types of NMR spectra can be equally successful, quantitatively analyzed. In Figs. 1 and 2, the optimal R_w ovals for these individual interresidual nOe and rOe build-up curve are plotted as functions of the ϕ,ψ dihedral angles on the basis of models A/B and A/B/C/D for **1** and **2**, respectively. Overlap has been accounted for to calculate the optimal R_w ovals. Each oval represents a predominant nOe or rOe intensity of one interresidual $^1H-^1H$ contact, as indicated in the figures. Therefore, in the case of overlap, more than one optimal R_w oval is present (e.g., Fig. 2(d) for the Man-**3** H-1,GlcNAc-**2** H-3/H-4/H-6pro*R* nOe and rOe in **2**). As a consequence, there are a few more optimal R_w ovals for the ROESY than for the NOESY data. Within the ovals the corresponding interresidual $^1H-^1H$ distances are (very) short, so the calculated nOe and rOe intensities within that ϕ,ψ area will be too large. Outside the ovals, the interresidual distances are large and the calculated nOe and rOe build-up curves are too small. Although the construction of the optimal R_w ovals depends on the model of the methyl glycoside, the optimal R_w ovals do facilitate the interpretation of the interresidual nOe and rOe build-up curves of the ϕ,ψ trajectories.

Conformational analysis of each glycosidic linkage.— The conformational properties of **1** and **2** will be discussed linkage by linkage. First, the MD trajectories are described. Subsequently, calculated nOe (and rOe) intensities from these trajectories will be compared with the experimental data. Finally, conclusions will be drawn with respect to the conformational characteristics of the linkage discussed.

The experimental and calculated interresidual nOe and rOe build up curves are shown in Fig. 3(a–e) for **1**

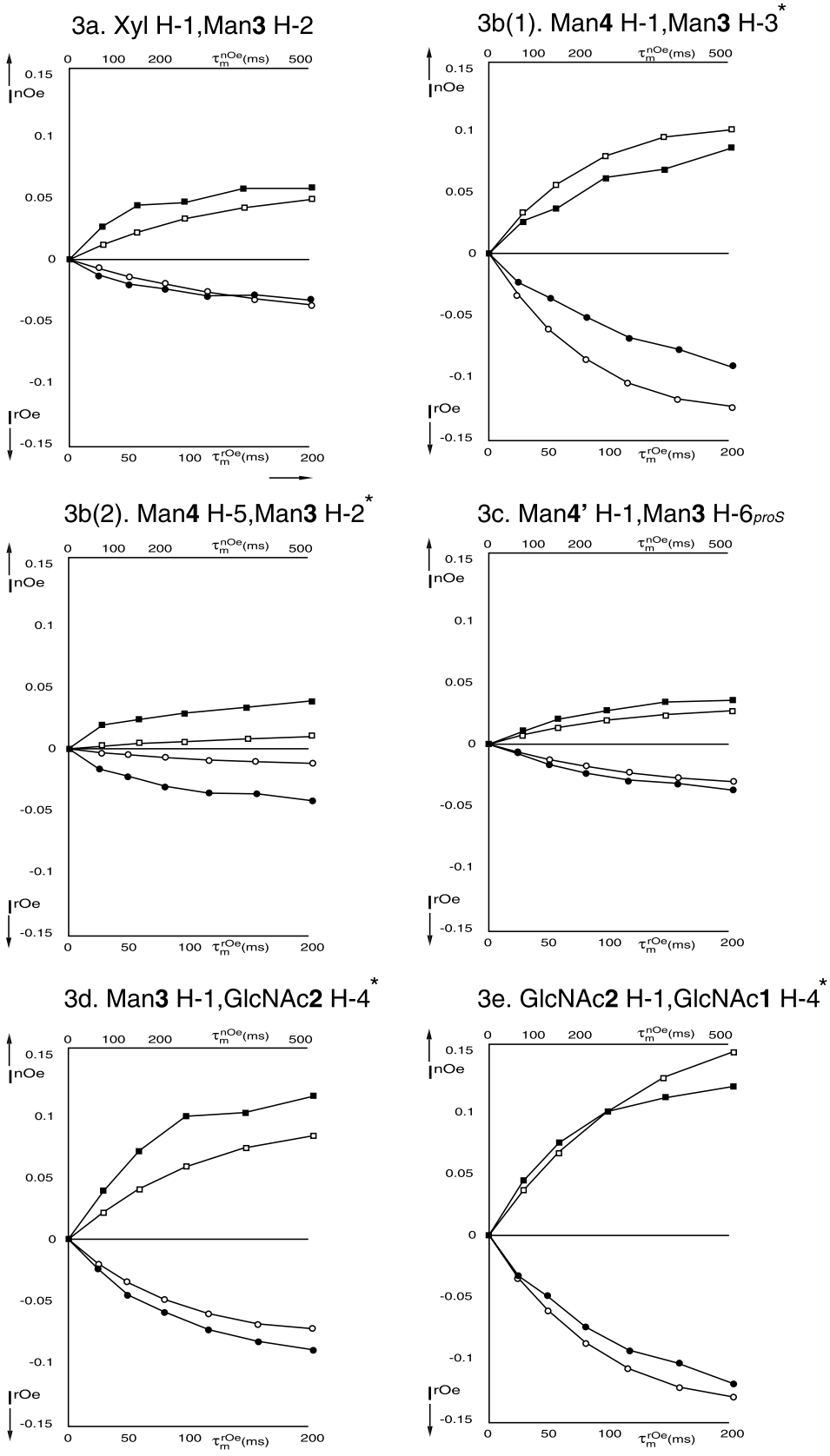

Fig. 3. Normalized build up curves of interresidual nOe's and rOe's of compound **1**, both experimental and calculated from data of the model A/B (calculation according to method IV in Ref. 27). nOe and rOe intensities are plotted as function of the mixing time (note the different mixing times for the nOe's and rOe's). Symbols used: ■, experimental nOe data; □, theoretical nOe data; ●, experimental rOe data; ○, theoretical rOe data. Build up curves marked with * represent normalized nOe and/or rOe data using overlap (Table 6).

Table 4
Stability of local minima at the glycosidic linkages, probed by short MD simulations for **1** and **2**

Glycosidic linkage	Compound **1**			Compound **2**		
	ϕ	ψ		ϕ	ψ	
Xyl-β-(1→2)-Man-**3**	−150	−150	s	−150	−150	ns
	40	−105	s	40	−105	ns
	−30	−70	ns	−80	−140	ns
Man-**4**-α-(1→3)-Man-**3**	170	−70	ns	170	−70	s
	60	170	ns	60	170	s
	90	90	s	90	90	s
				140	180	ns
Man-**4′**-α-(1→6)-Man-**3** (ω = −60°)	120	90	ns	120	90	s
	150	−110	ns	150	−110	ns
	140	165	s	140	−165	ns
	40	100	ns	160	100	ns
				100	150	ns
				40	180	ns
Man-**4′**-α-(1→6)-Man-**3** (ω = 60°)	140	100	s	140	100	ns
	160	−140	ns	160	−140	ns
	70	90	ns	100	140	s
	150	170	ns	180	120	ns
				60	40	ns
				180	40	ns
				80	−100	s
Man-**3**-β-(1→4)-GlcNAc-**2**	−90	−70	s	−120	70	s
	−130	70	ns	−130	−50	s
	−60	−30	s			
	−90	60	ns			
GlcNAc-**2**-β-(1→4)-GlcNAc-**1**	−60	−30	ns	−60	−30	s
	−90	80	ns	−90	80	s
	20	120	s	20	120	ns
				−90	−70	s
				80	60	s
Fuc-α-(1→6)-GlcNAc-**1** (ω = −60°)				−100	60	s
				−160	120	ns
				−20	−120	ns
				−60	120	s
Fuc-α-(1→6)-GlcNAc-**1** (ω = 60°)				−100	−80	s
				−140	−140	s
				−160	140	ns
				−160	40	ns
				−50	−70	s
				−60	−160	ns
				−80	100	ns

Criterion for a stable local minimum is a difference between starting and final conformation (after 50 ps simulation for **1** and 40 ps simulation for **2**) of less than 30° for both ϕ and ψ. Given are the starting ϕ,ψ values. s = stable; ns = not stable.

and Fig. 4(a–f) for **2**, wherein the calculated build up curves represent the combined models A/B and A/B/C/D for **1** and **2**, respectively. The calculated nOe and rOe build-up curves have very similar sizes and shapes, but the rOe build-up rate is higher, which is in agreement with the underlying physical principles.[8] As can be seen from Table 9, the interresidual nOe's and rOe's also give similar R_w values for the same theoretical models, and therefore, usually no distinction will be made between nOe and rOe data in the following conforma-

tional analysis. Both sets of experimental data will be evaluated in a separate paragraph.

*Xyl-β-(1→2)-Man-***3**.—The MD simulations of **1** point to a global minimum conformation $\phi,\psi = -80°, -95°$ for the linkage Xyl-β-(1→2)-Man-**3** (Fig. 1(a)). The difference in the average ϕ value of run A is about 10° from that of B, due to hydrogen bonding between Xyl O-2 and GlcNAc-**2** O-3, in total existing for 32% of the simulated time of A (Table 5). In **2** only the $\phi,\psi = -80°, -95°$ conformation is populated (Fig. 2(a)).

On the fast picosecond time scale, the mobility of the Xyl residue ($S_f^2 \approx 0.78$) is significantly less than that found in an analogous study for the Xyl-β-(1→2)-Man linkage in a glycopeptide glycan,[37] which lacks the Man-**4** residue ($S_f^2 \approx 0.6$). Apparently, the Man-**4** residue can cause a restriction of the mobility of the Xyl residue on this short time scale.

The calculated interresidual Xyl H-1,Man-**3** H-2 nOe intensities for the model A/B in **1** and A/B/C/D in **2**, fit the experimental data well (Figs. 3(a) and 4(a)). The local minimum at $\phi,\psi = 40°, -105°$ (see Fig. 1(a)) is not likely to exist for a considerable period of time, because this conformation does not contribute to the interresidual nOe intensities, as can be inferred from its position remote from the optimal R_w ovals. The local minimum at $\phi,\psi = -150°, -150°$ (Table 4) seems to be compatible with the experimental nOe data, as judged by the ovals. Although this minimum and the global minimum region are not separated by a large energy barrier (Figs. 1(a) and 2(a)), transitions between these minima do not happen in the MD simulation and there is no sign of a large internal motion, as can be seen from the slow-internal rotation correlation time ($\tau_{s,k}^{nOe/rOe} \approx 2.5/7.7$ ns in **1** and 3.0/7.5 ns in **2**, respectively, see also in 'Rotation correlation times'). Therefore, it is concluded that this linkage mainly adopts conformations in the $\phi,\psi = -80°, -95°$ region in both methyl glycosides.

*Man-***4**-*α-(1→3)-Man-***3**.—The MD simulations of the Man-**4**-α-(1→3)-Man-**3** linkage in **1** point to a global minimum at $\phi,\psi = 90°, -125°$ (Fig. 1(b)). These trajectories suggest a rather restricted conformation. However, in **2**, conformations also appear near $\phi,\psi = 70°, -150°$ and $130°, -90°$, respectively (Fig. 2(b)). In the disaccharide Man-α-(1→3)-Man, two important conformations have been found near $\phi,\psi = 100°, -90°$ and $\phi,\psi = 90°, -125°$,[38] respectively, between which transitions can be expected.[39] However, in **1** or **2** the conformation at $\phi,\psi = 100°, -90°$ is not possible, due to steric hindrance of the Xyl residue with Man-**4**. This observation is in agreement with earlier results,[40] pointing to the main minimum at $\phi,\psi = 100°, -90°$ for the Man-**4**-α-(1→3)-Man-**3** linkage in an N-glycan without Xyl, and to $\phi,\psi = 90°, -125°$ for this linkage in the same, but xylose-containing, N-glycan.

The optimal R_w ovals of the interresidual nOe's Man-**4** H-1,Man-**3** H-3 and Man-**4** H-5/H-2,Man-**3** H-2, have been plotted in Figs. 1(b) and 2(b). The calculated nOe intensities of Man-**4** H-1,Man-**3** H-3 are somewhat too large in **1**, but fit the experimental curves well in **2**. In both **1** and **2** the calculated build-up curves of Man-**4** H-5/H-2,Man-**3** H-2 are too small. However, the optimal R_w ovals for Man-**4** H-5/H-2,Man-**3** H-2 run through the simulated region. As the optimal R_w ovals are calculated by using HSEA geometries, it indicates a systematic difference between the Gromos and HSEA derived geometrics. Construction of this nOe is very sensitive for all geometric parameters, due to the large number of bonds and angles involved. As a

Table 5
Presence of hydrogen bonds [a] (% of the simulated trajectory) during the different long MD trajectories of **1** and **2**

Hydrogen bond		MD simulations of compound **1**		MD simulations of compound **2**			
Donor	···Acceptor	A	B	A	B	C	D
Man**4**′ O6	···GlcNAc**2** O3	25					14
Man**4**′ O6	···GlcNAc**2** C=O						50
Man**4**′ O6	···GlcNAc**2** O5						18
Man**4**′ O6	···GlcNAc**2** O4						5
Man**4**′ O4	···GlcNAc**2** C=O	8					
Man**4**′ O2	···GlcNAc**2** C=O						5
GlcNAc**2** O6	···Man**4**′ O4	8					
GlcNAc**2** O3	···Man**4**′ O6	11					
Xyl O2	···GlcNAc**2** O3	10					
GlcNAc**2** O3	···Xyl O2	22		10			
GlcNAc**2** O3	···Man**3** O5	33	14	24	11	6	51
GlcNAc**1** O3	···GlcNAc**2** O5	28	27	25	20	13	36
GlcNAc**2** N	···Fuc O2					42	

[a] Only hydrogen bonds are given which were formed for more than 5% of the complete MD trajectory.

Table 6
Relevant [a] clusters of proton resonances, which are treated as overlap in the CROSREL program, due to actual spectral overlap, as well as due to strong-relay TOCSY effects occurring in the ROESY experiments

Overlapping ^{1}H NMR resonances of compound **1**	
ROESY and NOESY spectra	ROESY spectra
Man-**4**′ H-2, Man-**3** H-6pro*R*	Xyl H-2, Xyl H-3
Man-**4** H-2, Man-**4** H-5	Man-**3** H-3, Man-**3** H-4
Xyl H-1, GlcNAc-**1** H-1	
GlcNAc-**2** H-2, GlcNAc-**2** H-3, GlcNAc-**2** H-4, GlcNAc-**2** H-6pro*R*	
GlcNAc-**1** H-5, GlcNAc-**1** OMe	
GlcNAc-**1** H-2, GlcNAc-**1** H-3, GlcNAc-**1** H-4, GlcNAc-**1** H-6pro*R*, GlcNAc-**2** H-5	

Overlapping ^{1}H NMR resonances of compound **2**		
ROESY and NOESY spectra	ROESY spectra	NOESY spectra
Man-**4**′ H-2, Man-**3** H-6pro*R*	Xyl H-2, Xyl H-3, GlcNAc-**1** OMe	Xyl H-3, GlcNAc-**1** OMe
Man-**4**′ H-1, Fuc H-1	Man-**3** H-3, Man-**3** H-4	GlcNAc-**1** H-3, GlcNAc-**1** H-5
Man-**4** H-2, Man-**4** H-5	GlcNAc-**1** H-2, GlcNAc-**1** H-3, GlcNAc-**1** H-5, GlcNAc-**2** H-5, GlcNAc-**1** H-6pro*R*	GlcNAc-**2** H-5, GlcNAc-**1** H-6pro*R*
Xyl H-1, GlcNAc-**1** H-1		
GlcNAc-**2** H-2, GlcNAc-**2** H-3, GlcNAc-**2** H-4, GlcNAc-**2** H-6pro*R*		
Fuc H-2, Fuc H-4		
Fuc H-3, GlcNAc-**1** H-6pro*S*		

[a] Meant are those cases of overlap, in which it is possible that a rOe/nOe contact might appear on the basis of a realistic three dimensional model of the involved oligosaccharide. For instance, the overlapping cross-peaks on the ROESY H-1 track of GlcNAc-**2**, i.e., Man-**4** H-4 (δ 3.632) and GlcNAc-**2** H-5 (δ 3.636), are *not* considered.

consequence, a small difference in ϕ,ψ will give rise to a large shift in R_w. Apparently, even the more detailed and comprehensive Gromos force field, and including the molecular dynamics, can only give an approximation of a true conformational behavior in solution. The fit of compound **2** is better, so it seems that the more broad distribution in (ϕ,ψ) describes the linkage better.

Due to the overlap of cross-peaks in the ROESY experiments, an extra R_w oval stemming from the Man-**4** H-1,Man-**3** H-4 contact appears, which made the low energy conformation at $\phi,\psi = 90°, 90°$ another alternative to the global minimum. As there was no Man-**4** H-1,Man-**3** H-4 cross-peak present in the NOESY spectrum, the $\phi,\psi = 90°, 90°$ conformation could be rejected.

The slow-internal rotation correlation time $\tau_{s,k}^{nOe/rOe}$ for this linkage is 3.8/9.3 ns in **1** and 6.6/12.7 ns in **2**, respectively. Although the ϕ,ψ values are found in a wide range in **2**, the long $\tau_{s,k}$ values point to rather slow transitions between the various minima, possibly caused by interference of the Xyl residue. The difference in distributions between **1** and **2** demonstrates that 1 ns of simulation is not sufficient to obtain a complete sampling of the ϕ,ψ space.

*Man-**4**′-α-(1→6)-Man-**3***.—The MD simulations of the Man-**4**′-α-(1→6)-Man-**3** linkage in **1** show trajectories located at different ϕ,ψ minima in the Man-**3** *gg* conformation ($\phi,\psi,\omega = 90°, -170°, -60°$; 150°, 180°, −60°; 80°, 100°, −60°, see Fig. 1(c1)). In **2**, similar areas for this $\omega = -60°$ rotamer are populated, except for the $\phi,\psi,\omega = 90°, -170°, -60°$ region. In the Man-**3** *gt* conformation, only the region $\phi,\psi,\omega =$ 90°, −170°, 60° is occupied in **1** (Fig. 1(c2)), whereas in **2** also another conformation exists at $\phi,\psi,\omega =$

Table 7
Local rotation correlation times (τ_k, ns) for the monosaccharide residues of compound **1** and compound **2** using method IV[27]

	Man-**4′** H-1,2 [a]	Man-**4** H-1,2	Xyl H-1,5_{ax}	Man-**3** H-1,2	GlcNAc-**2** H-1,3 [a]	GlcNAc-**1** H-1,3 [a]	Fuc H-1,2
Compound ***1***							
NOESY	0.60	0.81	0.73	1.03	0.97	0.90	
ROESY	0.29	0.96	0.94	1.07	1.30	1.17	
Compound ***2***							
NOESY	0.63	1.10	0.92	1.32	1.27	1.15	0.87
ROESY	0.32	0.77	0.92	0.82	1.26	1.19	0.77

The rotation correlation times were calculated using model A/B for compound **1** and model A/B/C/D for compound **2**, respectively, both derived from NOESY and ROESY spectra analysis.

[a] These intraresidual ^{1}H–^{1}H pairs contain overlap with other proton signals in the ROESY and NOESY spectra.

150°, 180°, 60°. Four different hydrogen bonds between Man-**4′** and GlcNAc-**2** have stabilized the single $\phi,\psi,\omega = 90°, -170°, 60°$ conformation in **1** (Table 5), whereas those hydrogen bonds have not been formed in **2**. This difference can result in a less restricted conformational behavior in that ϕ,ψ,ω region. In the scarcely populated $\phi,\psi,\omega = 105°, -85°, 60°$ conformation of **2** (Fig. 2(c2)), other hydrogen bonds between Man-**4′** and GlcNAc-**2** have been formed (Table 5). These hydrogen bonds originate entirely from MD simulation D, but seems unlikely to exist, as this conformation violates the Man-**4′** H-1,Man-**3** H-6pro*S* nOe intensities (Table 9, run D). In both **1** and **2**, the MD simulations do demonstrate the flexibility of the Man-**4′**-α-(1→6)-Man-**3** linkages, but they also point to the necessity of longer simulation times in order to sample the ϕ,ψ,ω space sufficiently. The considerable flexibility is also reflected in the small S_f^2 values across this linkage ($S_f^2 \approx 0.66$), and in the small slow-internal rotation correlation times ($\tau_{s,k}^{nOe/rOe} \approx 1.3/0.5$ ns).

The Man-**4′** H-1,H-2 nOe is the only available intraresidual nOe to which the local rotation correlation time τ_k of Man-**4′** can be fitted. In both **1** and **2**, the interresidual Man-**4′** H-1,Man-**3** H-6pro*R* nOe overlaps with this intraresidual nOe, and therefore, partially determines the fitted τ_k value. Another consequence of this overlap is that the conformations of the Man-**4′**-α-(1→6)-Man-**3** linkages can only be judged on basis of the Man-**4′** H-1,Man-**3** H-6pro*S* nOe intensities, which fit the theoretical data from the combined models A/B and A/B/C/D quite well (Figs. 3(c) and 4(c) for **1** and **2**, respectively). In both **1** and **2**, a *gg*/*gt* rotamer distribution of 7:3 exists, which have been derived from coupling constants (see '^{1}H and ^{13}C chemical shift assignments'). By consequence, the $\omega = 60°$ conformation contributes for 30% to the average proton–proton distances. From the NOESY spectra it is clear that no short Man-**4′** H-1,Man-**3** H-5 distance exists, and, as the $\phi,\psi,\omega = 80°, 100°, 60°$ conformation would contribute to that nOe contact, this conformation cannot exist for a significant period of time. It can be concluded that the conformational characteristics of the Man-**4′**-α-(1→6)-Man-**3** linkages in **1** and **2** are similar and that in both cases an ensemble of conformations mainly exists in the regions ϕ from 80° to 160° and ψ from 150° to 220°, however, the $\phi,\psi,\omega = 80°, 100°, -60°$ conformation cannot be excluded.

*Man-**3**-β-(1→4)-GlcNAc-**2***.—The MD simulations of the linkage Man-**3**-β-(1→4)-GlcNAc-**2** point to a global minimum conformation in the region $\phi,\psi = -65°, 110°$ (Figs. 1(d) and 2(d)). The global minimum is stabilized by a single hydrogen bond between GlcNAc-**2** O-3 and Man-**3** O-5 (23% and 24% in **1** and **2**,

Table 8
Slow-internal rotation correlation times ($\tau_{s,k}$, ns) for the glycosidic linkages of **1** and of **2**, as calculated from local rotation correlation times (τ_k) using method IV and model A/B for **1** and model A/B/C/D for **2**, derived from NOESY and ROESY spectra analysis

Linkage	Compound **1**		Compound **2**	
	NOESY	ROESY	NOESY	ROESY
Man-**4′**-α-(1→6)-Man-**3** [a]	1.4	0.4	1.2	0.5
Man-**4**-α-(1→3)-Man-**3**	3.8	9.3	6.6	12.7
Xyl-β-(1→2)-Man-**3**	2.5	7.7	3.0	7.5
Man-**3**-β-(1→4)-GlcNAc-**2**	16.7	6.0	33.5	2.3
GlcNAc-**2**-β-(1→4)-GlcNAc-**1**	12.5	11.7	12.2	21.4
Fuc-α-(1→6)-GlcNAc-**1**	n/a	n/a	3.6	2.2

[a] Determination of the slow-internal rotation correlation time for this linkage was conformation-dependent.

Table 9
R_w values [a] for individual interresidual nOe and rOe intensities of the glycosidic linkages of compound **1** and compound **2**, applying Method IV[27]

Traj./model	All	Man-**4**′ H-1 Man-**3** H-6pro*S*	Man-**4** H-1 Man-**3** H-3/H-4	Man-**4** H-5/H-2 Man-**3** H-2	Xyl H-1 Man-**3** H-2	Man-**3** H-1 GlcNAc-**2** H-3,4,6pro*R*	GlcNAc-**2** H-1 GlcNAc-**1** H-4	Fuc H-1 GlcNAc-**1** H-6pro*S*	Fuc H-1 GlcNAc-**1** H-6pro*R*	Fuc H-1 GlcNAc-**2** H-1
	Compound **1**									
	NOESY									
A	0.262	−0.299	+0.212	n.d.	−0.305	−0.326	±0.195			
B	0.272	−0.275	+0.187	n.d.	−0.365	−0.362	±0.145			
A/B	0.287	−0.273	+0.319	n.d.	−0.348	−0.350	±0.159			
	ROESY									
A	0.432	−0.285	+0.455	−0.776	±0.150	−0.103	+0.173			
B	0.385	−0.160	+0.496	−0.759	±0.169	−0.255	+0.154			
A/B	0.368	−0.188	+0.532	−0.759	±0.148	−0.184	+0.157			
	Compound **2**									
	NOESY									
A	0.393	+0.173	+0.332	−0.806	±0.098	−0.275	−0.242	+1.080	−0.453	−0.861
B	0.318	+0.264	−0.279	−0.601	+0.244	+0.087	−0.215	−0.324	+0.829	−0.898
C	0.521	+0.598	−0.226	−0.676	+1.648	−0.119	+0.254	±0.051	+0.156	−0.881
D	0.564	−0.896	+0.648	−0.770	+1.155	−0.268	+0.272	+0.577	−0.180	−0.910
A/B/C/D	0.276	+0.223	−0.133	−0.785	+0.144	±0.042	+0.091	±0.075 [b]	+0.265 [b]	−0.739 [b]
	ROESY									
A	0.825	±0.280	+0.445	−0.844	+0.286	−0.127	−0.221	+3.459	−0.573	−0.838
B	0.568	+0.287	−0.229	−0.712	+0.243	+0.313	−0.170	−0.696	+1.168	−0.961
C	0.408	±0.077	+0.224	−0.849	±0.066	+0.237	+0.479	±0.104	+0.493	−0.600
D	0.817	−0.991	+0.648	−0.839	+1.123	−0.210	+0.104	+2.368	−0.155	−0.966
A/B/C/D	0.422	±0.081	+0.220	−0.827	±0.169	±0.124	+0.102	+0.311 [b]	+0.444 [b]	−0.698 [b]

[a] Minus, plus and minus/plus shows if the calculated build up curve is respectively smaller, larger or goes through the experimental measured curve, respectively.
[b] Calculated without using the first 200 ps of MD simulation A

respectively). The conformation near $\phi,\psi = -50°, 150°$ in **1** is present for a short period of time during MD simulation A. The last conformation is stabilized by the hydrogen bond between Xyl O-2 and GlcNAc-**2** O-3 (Table 5).

The optimal R_w ovals for Man-**3** H-1,GlcNAc-**2** H-3/H-4/H-6pro*R* are plotted in Figs. 1(d) and 2(d) for **1** and **2**, respectively. The ω dihedral angle of GlcNAc-**2** determines largely the distance between Man-**3** H-1 and GlcNAc-**2** H-6pro*R*. Only the GlcNAc-**2** $\omega = -60°$ rotamer results in a short distance, which, therefore, mainly contributes to the Man-**3** H-1,GlcNAc-**2** H-6pro*R* nOe. During the MD simulations of both **1** and **2**, GlcNAc-**2** was found in the $\omega = -60°$ conformation only, favoring the Man-**3** H-1,GlcNAc-**2** H-6pro*R* nOe intensity. As there exists a *gg*/*gt* rotamer distribution for GlcNAc-**2** (*gg*:*gt* = 3:2, derived from coupling constants), the calculated interresidual nOe intensities have been somewhat overestimated. Note that the proper *gg*:*gt* distribution would actually lead to slightly worse fits to the experimental nOe build up curves, than are presented in Figs. 3(d) and 4(d) for **1** and **2**, respectively.

The local minimum at $\phi,\psi = 20°, 120°$ (Figs. 1(d) or 2(d)) is not possible, due to steric hindrance between GlcNAc-**2** and Xyl. The other local minima at $\phi,\psi = -90°, -70°$ and $-60°, -30°$, respectively (Table 4), might strongly contribute to the observed interresidual nOe, because of a short Man-**3** H-1,GlcNAc-**2** H-3 distance (Figs. 1(d) and 2(d)). The glycosidic linkages of GlcNAc-**2**-β-(1→4)-GlcNAc-**1** and Man-**3**-β-(1→4)-GlcNAc-**2** and of methyl cellobioside[6] have similar micro-environments and, by consequence, have resembling iso-energy contour plots (see Figs. 1(d, e) and 2(d, e)). The $\phi,\psi = -90°, -70°$ and $-60°, -30°$ local minima at the GlcNAc-**2**-β-(1→4)-GlcNAc-**1** linkage

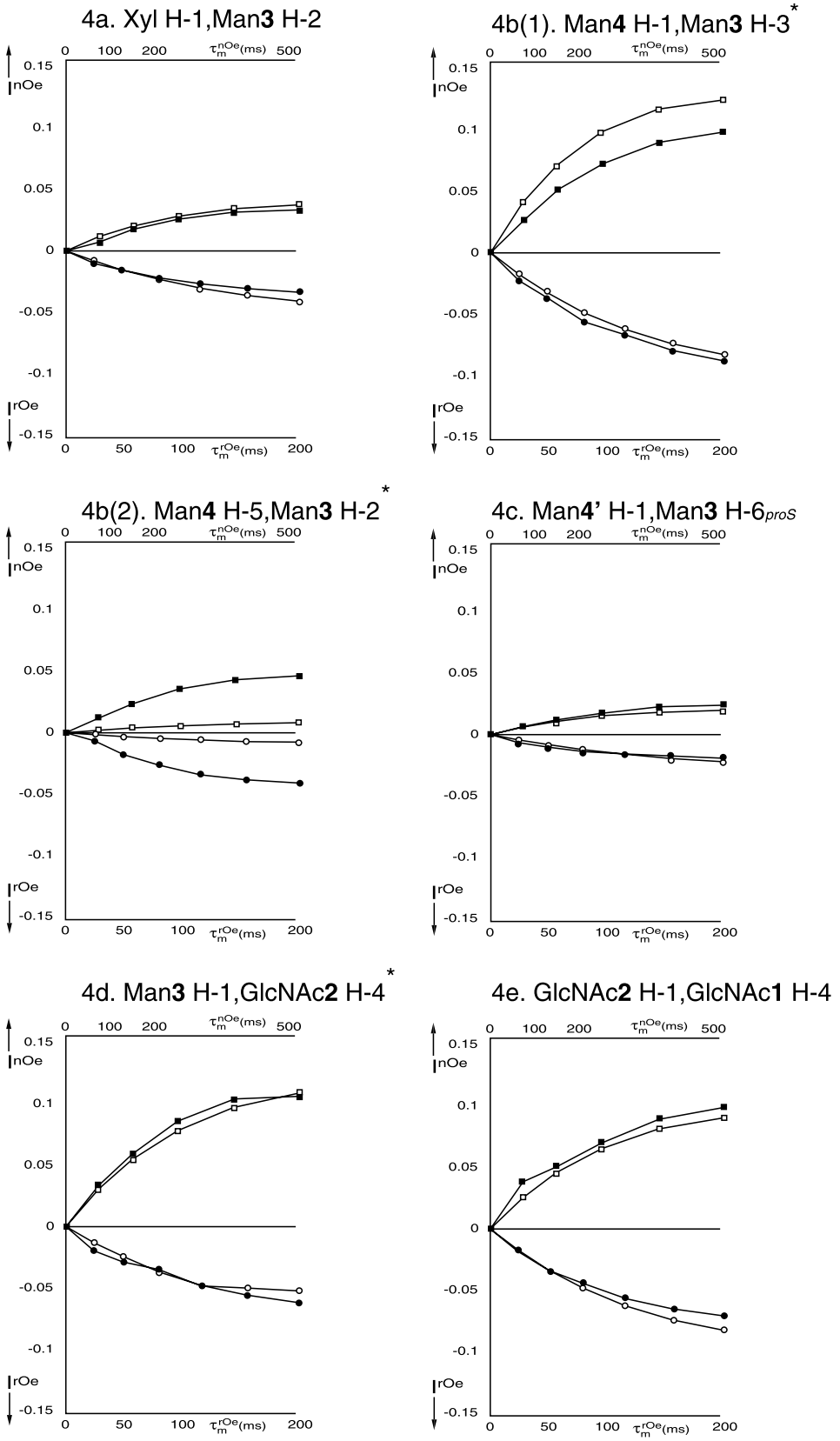

Fig. 4. Normalized build up curves of interresidual nOe's and rOe's of compound **2**, both experimental and calculated from data of the model A/B/C/D (calculation according to method IV in Ref. 27). NOe and rOe intensities are plotted as function of the mixing time. Symbols as used in Fig. 3. Build up curves marked with * represent normalized nOe and/or rOe data using overlap (Table 6).

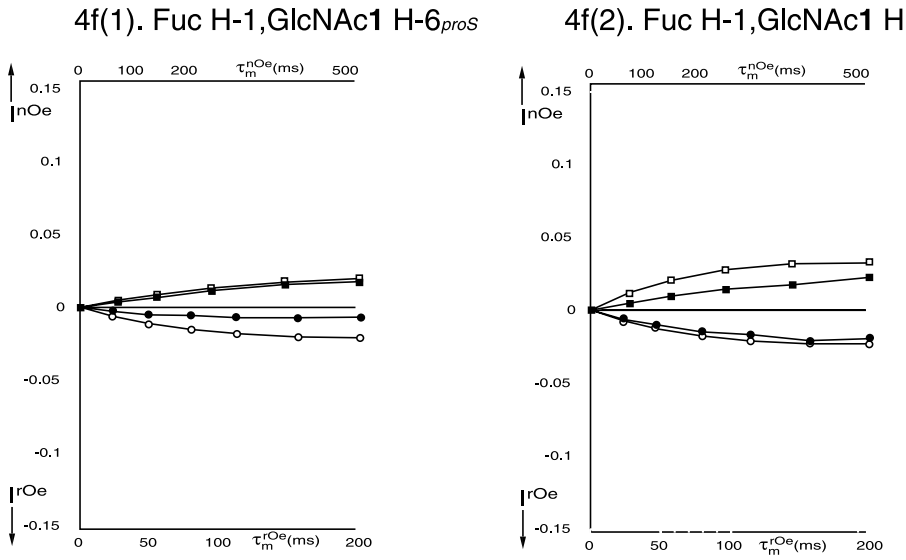

Fig. 4. (*Continued*)

do not exist for a considerable period of time (see below), and in methyl cellobioside these conformations are probably non-existent.[6] Therefore, it is concluded for **1** and **2** that the $\phi,\psi = -90°, -70°$ and $-60°, -30°$ conformations are not present for a significant period of time.

At the Man-**3**-β-(1→4)-GlcNAc-**2** linkage there are no signs of conformational transitions, as inferred from the long slow-internal rotation correlation times ($\tau_{s,k}^{nOe/rOe} \approx 16.7/6.0$ and 33.5/2.3 ns for **1** and **2**, respectively). The mobility of this linkage is also restricted on the picosecond time scale ($S_f^2 \approx 0.84$). Thus, the global minimum, enhanced by the hydrogen bond between Man-**3** O-5 and GlcNAc-**2** O-3, is the predominant and rather rigid, conformation of this linkage.

*GlcNAc-**2**-β-(1→4)-GlcNAc-**1***.—The MD simulations indicate that the global minimum of the linkage GlcNAc-**2**-β-(1→4)-GlcNAc-**1** is at $\phi,\psi = -70°, 110°$. As for the Man-**3**-β-(1→4)-GlcNAc-**2** linkage, the conformation is stabilized by the hydrogen bond between GlcNAc-**1** O-3 and GlcNAc-**2** O-5 (28% in **1** and 27% in **2**, respectively).

The optimal R_w ovals for GlcNAc-**2** H-1,GlcNAc-**1** H-3/H-4/H-6pro*R* in **1** are plotted in Fig. 1(e). For similar reasons as for the Man-**3**-β-(1→4)-GlcNAc-**2** linkage, the $\phi,\psi = -90°, -70°$ and $-60°, -30°$ conformations probably do not exist, nor the local minimum conformation $\phi,\psi = 20°, 120°$, which turns out to be unstable in methyl cellobioside.[6] The GlcNAc-**1** H-4 signal has a well-resolved position in the proton spectrum of **2** as a consequence of the α-(1→6)-linked fucose residue to GlcNAc-**1**. Therefore, only one R_w oval is present in the ϕ,ψ plot (Fig. 4(e)). This single optimal R_w oval does not run through any of the three aforementioned local minima, and therefore, these local minima do not exist for a significant period of time.

The $\tau_{s,k}$ values corresponding to this linkage in **1** ($\tau_{s,k}^{nOe/rOe} \approx 12.5/11.7$ ns) point to a rather rigid linkage. Although at larger $\tau_{s,k}$ values, this value becomes less precise, the $\tau_{s,k}^{nOe/rOe}$ in **2** ($\tau_{s,k}^{nOe/rOe} \approx 12.2/21.4$ ns) indicate that the GlcNAc-**2**-β-(1→4)-GlcNAc-**1** linkage is even more rigid in **2**. This can be due to (i) the interaction of the Fuc residue with GlcNAc-**2** (see below) and/or (ii) the higher mass of the Fuc-α-(1→6)-GlcNAc-**1** disaccharide in comparison with the GlcNAc-**1** residue only. Nevertheless, the results indicate the predominant existence of a single conformation at the global minimum $\phi,\psi = -70°, 110°$ of the GlcNAc-**2**-β-(1→4)-GlcNAc-**1** linkage both in **1** and in **2**, thus being very similar to that of the Man-**3**-β-(1→4)-GlcNAc-**2** linkage.

*Fuc-α-(1→6)-GlcNAc-**1***.—The difference in primary structure between **1** and **2** is the additional Fuc residue in **2**, which is α-(1→6) linked to GlcNAc-**1**. The MD trajectories of the Fuc-α-(1→6)-GlcNAc-**1** linkage demonstrate flexibility of this linkage (Fig. 2(f1) and (f2), respectively). The highest populated region is at $\phi,\psi = -95°, 175°$ for both the GlcNAc-**1** *gg* and *gt* conformations. In the *gg* rotamer the Fuc residue bends towards GlcNAc-**2**, and makes the hydrogen bond between Fuc O-2 and GlcNAc-**2** N-H possible (43% of the simulated time in trajectory C, Table 5). In the *gt* conformation, Fuc turns away from GlcNAc-**2**. HSEA calculations point to the energetically favorable conformation at $\phi,\psi = -100°, 110°$ in the *gg* conformation of GlcNAc-**1** (Fig. 4(f1)). Although this conformation turned out to be stable for about 200 ps during MD simulation A, the calculated interresidual nOe intensities for this conformation violate the experimental data. Therefore, this conformation can exist only for a small period of time.

The optimal R_w ovals are plotted in Fig. 2(f1) and (f2) for the three interresidual nOe's: Fuc H-1 interact-

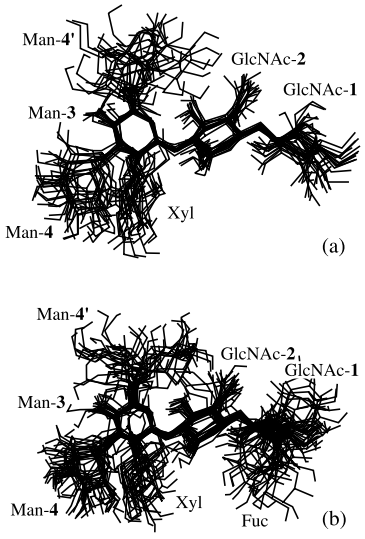

Fig. 5. Superimposed conformations on the β-D-Man-**3**-(1→4)-β-D-GlcNAc-**2**-(1→4)-β-D-GlcNAc-**1** element appearing during the MD simulations. (a) Compound **1**; (b) compound **2**.

ing with GlcNAc-**1** H-6pro*R*, GlcNAc-**1** H-6pro*S* and GlcNAc-**2** H-1, respectively. The observed Fuc H-1,GlcNAc-**2** H-1 nOe is only possible in the *gg* conformation of GlcNAc-**1** ($gg:gt = 65:35$ for the Fuc-α-(1→6)-GlcNAc-**1** linkage, see '^{1}H and ^{13}C chemical shift assignments'). This cross-peak, present in the NOESY, as well as in the ROESY spectra, is very weak. The size and the position of the corresponding optimal R_w oval is uncertain, as they depend on eight covalent bonds, seven valence angles and five freely rotatable dihedral angles between Fuc H-1 and GlcNAc-**2** H-1 (see also the Man-**4** H-5/H-2,Man-**3** H-2 nOe). The calculated Fuc H-1,GlcNAc-**2** H-1 nOe build-up curve is too weak in all cases. Only the $\phi,\psi,\omega = -70°, -100°, -60°$ low energy region can result in a short Fuc H-1,GlcNAc-**2** H-1 distance, which can strongly contribute to the intensity of this nOe.

In conclusion, the Fuc-α-(1→6)-GlcNAc-**1** linkage is flexible, which is confirmed by the short $\tau_{s,k}$ ($\tau_{s,k}^{nOe/rOe} \approx$ 3.6/2.2 ns), by the small generalized order parameters across this linkage ($S_f^2 \approx 0.72$) and by the nOe data that point to the presence of an ensemble of conformations in the region from $\phi = 200°$ to 320° and $\psi = 160°$ to 300°.

Assessment of NOESY and ROESY analysis.—The NOESY and ROESY spectra contain the identical information, which is related to average conformations in solution and can be analyzed quantitatively. The combination of data derived from these NMR experiments and MD simulations in water results in a powerful method to describe the conformational behavior of an oligosaccharide chain in the biologically relevant, aqueous environment. However, there are differences between NOESY and ROESY data, which may effect the analysis.

ROESY data can be corrected for typical effects such as offset dependency, spin-lock field strength and TOCSY transfers. However, due to these relay TOCSY effects, the number of cross-peaks which have to be treated as overlap can be much larger than for the NOESY analysis. In the case of oligosaccharide chains, where many protons resonate at about the same frequencies and have large joint scalar coupling constants, the occurrence of strong relay TOCSY effects can be considerable, both in magnitude and in frequency. Examples are the 'overlapping' Xyl H-2,Xyl H-3, GlcNAc-**2** H-2,GlcNAc-**2** H-3 (in **2**) and Man-**3** H-3,Man-**3** H-4.

Nevertheless, both ^{1}H–^{1}H NOESY and ^{1}H–^{1}H ROESY spectra suffer from a lot of overlap in (oligo)saccharide spectra as most protons resonate in a small spectral area ($\sim$4.0–3.5 ppm). Generally, this causes the analysis to be less accurate, as the conformational data obtained become less specific. For example, overlap of Man-**4**′ H-2 with Man-**3** H-6pro*R* has complicated the analysis at the Man-**4**′-α-(1→6)-Man-**3** linkage.

4. Conclusion

The conformational behavior of two closely related methyl glycosides **1** and **2** have been characterized on basis of MD simulations in water and (rotating frame) nuclear Overhauser enhancement spectroscopy. The mobility of each glycosidic linkage has been described in terms of: (i) the ϕ,ψ space covered by the MD simulations and its consistency with the measured inter-residual nOe intensities; (ii) the generalized order parameters S_f^2, derived from MD simulations, which are a measure of fast motions on the picosecond time scale; (iii) the slow-internal rotation correlation times $\tau_{s,k}$ which indicate the frequency of transitions between the favorable regions in the ϕ,ψ space.

It can be concluded that the common part of **1** and **2**, which is **1**, has the same conformation. Each linkage in the β-D-Xyl-(1→2)-β-D-Man-(1→4)-β-D-GlcNAc-(1→4)-β-D-GlcNAc fragment populates only one single region of the ϕ,ψ space. If conformational transitions occur in this tetrasaccharide part of both molecules at all, then this happens on a time scale significantly longer than that of the overall rotation of the molecule (> 1 ns). The MD simulations demonstrate flexibility at the α-D-Man-(1→3)-β-D-Man, α-D-Man-(1→6)-β-D-Man and α-L-Fuc-(1→6)-β-D-GlcNAc glycosidic linkages. This has been visualized in Fig. 5(a) for **1** and in Fig. 5(b) for **2**, by superposition of simulated conformations. The comparisons of calculated nOe or rOe intensities with the experimental data point to a set of

conformations present for these linkages, because single conformations do not explain the experimental intensities, whereas the sets do. In case of the α-D-Man-(1→3)-β-D-Man linkage the slow-internal rotation correlation times $\tau_{s,k}$ show that the rate of large conformational transitions is relatively small at this linkage, whereas the $\tau_{s,k}$ for the α-D-Man-(1→6)-β-D-Man and α-L-Fuc-(1→6)-β-D-GlcNAc linkages indicate high transition rates at these linkages. High mobilities on the picosecond time scale, as inferred from the generalized order parameter S_f^2, are mainly found at the α-(1→6) linkages. It is interesting to observe that both the Man and Fuc residues at these α-(1→6) linkages have the possibility to bend towards the inner core, where these residues can interact with GlcNAc-**2** (Fig. 5(a) and (b)). Alternatively, these residues can turn away from the center of the methyl glycoside, and, by consequence, the methyl glycoside can occupy a large area in conformational space.

Different φ,ψ trajectories in identical micro-environments have been simulated for glycosidic linkages of the α-D-Man-(1→6)-[α-D-Man-(1→3)-]β-D-Man part in **1** and **2**. Both the α-D-Man-(1→6)-β-D-Man and α-D-Man-(1→3)-β-D-Man linkages turned out to be flexible. However, the slow-internal rotation correlation times indicate that transitions for the Man-α-(1→6)-Man linkage ($\tau_{s,k} \approx 1$ ns) happen about 7 times more frequently than for the Man-α-(1→3)-Man linkage ($\tau_{s,k} \approx 8$ ns). From this, and a previous study,[10] it appears that especially in the cases of flexible linkages, in which conformational transitions occur at a nanosecond time scale, a simulation time of at least several times the characteristic time of conformational transitions of the glycosidic linkages is required in order to obtain adequate sampling.

Although both $^1H-^1H$ NOESY and $^1H-^1H$ ROESY spectra suffer from overlap, $^1H-^1H$ NOESY should be the method of choice to obtain experimental data for the conformational analysis of oligosaccharides. On the other hand, ROESY experiments are extremely powerful in those cases when NOESY experiments hardly provide the conformational data needed. This is the case for medium-sized molecules where $\omega\tau_c \sim 1$, such as for disaccharides.[6,8]

Acknowledgements

This investigation was financially supported by the Council for Chemical Sciences (CW) of the Netherlands Organization for Scientific Research (NWO). We thank the authors of GROMOS for the use of their program package.

References

1. Rice, K. G.; Wu, P.; Brand, L.; Lee, Y. C. *Curr. Opin. Struct. Biol.* **1993**, *3*, 669–674.
2. Pérez, S. *Curr. Opin. Struct. Biol.* **1993**, *3*, 675–680.
3. Rutherford, T. J.; Partridge, J.; Weller, C. T.; Homans, S. W. *Biochemistry* **1993**, *32*, 12715–12724.
4. Edge, C. J.; Singh, U. C.; Bazzo, R.; Taylor, G. L.; Dwek, R. A.; Rademacher, T. W. *Biochemistry* **1990**, *29*, 1971–1974.
5. Cumming, D. A.; Carver, J. P. *Biochemistry* **1987**, *26*, 6664–6676.
6. Kroon-Batenburg, L. M. J.; Kroon, J.; Leeflang, B. R.; Vliegenthart, J. F. G. *Carbohydr. Res.* **1993**, *245*, 21–45.
7. Jiménez Blanco, J. L.; van Rooijen, J. J. M.; Erbel, P. J. A.; Leeflang, B. R.; Kamerling, J. P.; Vliegenthart, J. F. G. *J. Biomol. NMR* **2000**, *16*, 59–77.
8. Leeflang, B. R.; Kroon-Batenburg, L. M. J. *J. Biomol. NMR* **1992**, *2*, 495–518.
9. Neuhaus, D.; Williamson, M. *The Nuclear Overhauser Effect in Structural and Conformational Analysis*; VCH: New York, 1989; pp 312–327.
10. Lommerse, J. P. M.; Kroon-Batenburg, L. M. J.; Kroon, J.; Kamerling, J. P.; Vliegenthart, J. F. G. *J. Biomol. NMR* **1995**, *5*, 79–94.
11. Van Kuik, J. A.; van Halbeek, H.; Kamerling, J. P.; Vliegenthart, J. F. G. *J. Biol. Chem.* **1985**, *260*, 13984–13988.
12. Lommerse, J. P. M.; Thomas-Oates, J. E.; Gielens, C.; Préaux, G.; Kamerling, J. P.; Vliegenthart, J. F. G. *Eur. J. Biochem.* **1997**, *249*, 195–222.
13. Van der Ven, J. G. M.; Kerékgyártó, J.; Kamerling, J. P.; Lipták, A.; Vliegenthart, J. F. G. *Carbohydr. Res.* **1994**, *264*, 45–62.
14. Vliegenthart, J. F. G.; Dorland, L.; van Halbeek, H. *Adv. Carbohydr. Chem. Biochem.* **1983**, *41*, 209–374.
15. Bax, A.; Davis, D. G. *J. Magn. Reson.* **1985**, *65*, 355–360.
16. Macura, S.; Ernst, R. R. *J. Magn. Reson.* **1983**, *53*, 521–528.
17. Bax, A.; Davis, D. G. *J. Magn. Reson.* **1985**, *63*, 207–213.
18. Marion, D.; Wüthrich, K. *Biochem. Biophys. Res. Commun.* **1983**, *117*, 479–485.
19. Bax, A.; Griffey, R. H.; Hawkins, B. L. *J. Magn. Reson.* **1983**, *55*, 301–315.
20. Garbow, J. R.; Weirekamp, D. P.; Pines, A. *Chem. Phys. Lett.* **1982**, *93*, 504–509.
21. Olejniczak, E. T.; Eaton, H. E. *J. Magn. Reson.* **1990**, *87*, 628–632.
22. Press, W. H.; Flannery, B. P.; Teukolsky, S. A.; Vetterling, W. T. *Numerical Recipes*; Cambridge University Press: Cambridge, 1986 Ch. 12.
23. Stuike-Prill, R.; Meyer, B. *Eur. J. Biochem.* **1990**, *194*, 903–919.
24. Kitaygorodsky, A. I. *Chem. Soc. Rev.* **1978**, *7*, 133–163.
25. IUPAC-IUB Joint Commission on Biochemical Nomenclature (JCBN), *Eur. J. Biochem.* **1983**, *131*, 5–7.
26. Tran, V.; Buleon, A.; Imberty, A.; Pérez, S. *Biopolymers* **1989**, *28*, 679–690.
27. French, A. D. *Carbohydr. Res.* **1989**, *188*, 206–211.
28. Van Gunsteren, W. F. *GROMOS*, *Groningen Molecular Simulation Package*; University of Groningen: The Netherlands, 1987.
29. Lommerse, J. P. M.; Kroon-Batenburg, L. M. J.; Kamerling, J. P.; Vliegenthart, J. F. G. *Biochemistry* **1995**, *34*, 8196–8206.

30. Van Gunsteren, W. F.; Berendsen, H. J. C. *Mol. Phys.* **1977**, *34*, 1311–1327.
31. Van Eijck, B. P.; Kroon, J. *J. Mol. Struct.* **1989**, *195*, 133–146.
32. Nishida, Y.; Hori, H.; Ohrui, H.; Meguro, H. *Carbohydr. Res.* **1987**, *170*, 106–111.
33. Hori, H.; Nishida, Y.; Ohrui, H.; Meguro, H.; Uzawa, J. *Tetrahedron Lett.* **1988**, *29*, 4457–4460.
34. Haasnoot, C. A. G.; de Leeuw, F. A. A. M.; Altona, C. *Tetrahedron* **1979**, *36*, 2783–2792.
35. Lhernould, S.; Karamanos, Y.; Bourgerie, S.; Strecker, G.; Julien, R.; Morvan, H. *Glycoconjugate J.* **1992**, *9*, 191–197.
36. Baumann, H.; Jansson, P.-E.; Kenne, L. *J. Chem. Soc., Perkin Trans. I* **1991**, 2229.
37. Homans, S. W.; Pastore, A.; Dwek, R. A.; Rademacher, T. W. *Biochemistry* **1987**, *26*, 6649–6655.
38. Imberty, A.; Gerber, S.; Tran, V.; Pérez, S. *Glycoconjugate J.* **1990**, *7*, 27–54.
39. De Waard, P.; Leeflang, B. R.; Vliegenthart, J. F. G.; Boelens, R.; Vuister, G. W.; Kaptein, R. *J. Biomol. NMR* **1992**, *2*, 211–226.
40. Homans, S. W.; Dwek, R. A.; Rademacher, T. W. *Biochemistry* **1987**, *26*, 6553–6560.